Lattice Boltzmann model for axisymmetric multiphase flows

Kannan N. Premnath* and John Abraham†
M.J. Zucrow Labs., School of Mechanical Engineering, Purdue University, West Lafayette, Indiana 47907, USA
(Received 28 October 2004; published 25 May 2005)

A lattice Boltzmann model is presented for axisymmetric multiphase flows. Source terms are added to a two-dimensional standard lattice Boltzmann equation for multiphase flows such that the emergent dynamics can be transformed into the axisymmetric cylindrical coordinate system. The source terms are temporally and spatially dependent and represent the axisymmetric contribution of the order parameter of fluid phases and inertial, viscous, and surface tension forces. A model which is effectively explicit and second order is obtained. This is achieved by taking into account the discrete lattice effects in the Chapman-Enskog multiscale analysis, so that the macroscopic axisymmetric mass and momentum equations for multiphase flows are recovered self-consistently. The model is extended to incorporate reduced compressibility effects. Axisymmetric equilibrium drop formation and oscillations, breakup and formation of satellite droplets from viscous liquid cylindrical jets through Rayleigh capillary instability, and drop collisions are presented. Comparisons of the computed results with available data show satisfactory agreement.

DOI: 10.1103/PhysRevE.71.056706 PACS number(s): 47.11.+j, 47.55.Kf, 05.20.Dd, 47.55.Dz

I. INTRODUCTION

Fluid flow with interfaces and free surfaces is common in nature and in many engineering applications. Such interfacial flows which typically involve multiple scales remain a formidable nonlinear problem rich in physics and continue to pose challenges to experimentalists and theoreticians alike [1]. Numerical simulation of multiphase flows is challenging as the shape and location of the interfaces must be computed in conjunction with the solution of the flow field [2,3]. Computational methods based on the lattice Boltzmann equation (LBE) for simulating complex emergent physical phenomena have attracted much attention in recent years [4,5]. The LBE simulates multiphase flows by incorporating interfacial physics at scales smaller than macroscopic scales. Phase segregation and interfacial fluid dynamics can be simulated by incorporating interparticle potentials [6,7], concepts based on free energy [8,9], or kinetic theory of dense fluids [10–12].

The formulation of the standard LBE is based on the Cartesian coordinate system and does not take into account axial symmetry, which may exist. Numerous multiphase flow situations exist where the fluid dynamics can be approximated as axisymmetric [1,13]. Examples include head-on collision of drops, normal drop impingement on solid surfaces, and Rayleigh instability of cylindrical liquid columns. Currently, full three-dimensional (3D) calculations have to be carried out for problems which may be approximated as axisymmetric [14–16]. In 3D computations, computational considerations restrict the numerical resolution that may be employed and the physics may not be well resolved. For example, in the breakup of drops into satellite droplets the size of the droplets may be such that the 3D grids may not resolve them. To improve the computational efficiency of the LBE for axisymmetric multiphase flows, we propose an axisymmetric LB model in this paper. The approach consists of adding source terms to the 2D Cartesian LBE model based on the kinetic theory of dense fluids for multiphase flows [10,11]. This approach is similar in spirit to the idea proposed in [17] to solve single-phase axisymmetric flows. However, multiphase flow problems involve additional complexity as a result of interfacial physics involved—i.e., the surface tension forces and the need to track the interfaces. In this case, the accuracy of the numerical discretization of the source terms representing interfacial physics also becomes an important consideration.

This paper is organized as follows. In Sec. II, the axisymmetric LBE multiphase model is described. Then, in Sec. III, its extension to simulate axisymmetric multiphase flows with reduced compressibility effects is described. The computational methodology adopted is also discussed in this section. In Sec. IV, the axisymmetric model is applied to benchmark problems to evaluate its accuracy. Finally, the paper closes with a summary in Sec. V.

II. AXISYMMETRIC LBE MULTIPHASE FLOW MODEL

To simulate axisymmetric multiphase flows, axisymmetric contributions of the order parameter and inertial, viscous, and surface tension forces may be introduced to the standard 2D LBE. The source terms, which will be shown to be spatially and temporally dependent, are determined by performing a Chapman-Enskog multiscale analysis in such a way that the macroscopic mass and momentum equations for multiphase flows are recovered self-consistently. The introduction of source terms makes it necessary to calculate additional spatial gradients when compared to those in the standard LBE. While this approach is developed for a specific LBE multiphase flow model based on kinetic theory of dense fluids [10,11], it can be readily extended to other LBE multiphase flow models.

The governing continuum equations of isothermal multiphase flow [18,19] in the cylindrical coordinate system when

*Electronic address: nandha@ecn.purdue.edu
†Electronic address: jabraham@ecn.purdue.edu

the axisymmetric assumption is employed are

$$\partial_t \rho + \frac{1}{r}\partial_r(\rho r u_r) + \partial_z(\rho u_z) = 0, \tag{1}$$

$$\rho(\partial_t u_r + u_r\partial_r u_r + u_z\partial_z u_r) = -\partial_r P + F_{s,r} + F_{ext,r} + \frac{1}{r}\partial_r(r\Pi_{rr}) + \partial_z(\Pi_{rz}), \tag{2}$$

$$\rho(\partial_t u_z + u_r\partial_r u_z + u_z\partial_z u_z) = -\partial_z P + F_{s,z} + F_{ext,z} + \frac{1}{r}\partial_r(r\Pi_{zr}) + \partial_z(\Pi_{zz}), \tag{3}$$

where ρ is the density and u_r and u_z are the radial and axial components of velocity. These equations are derived from kinetic theory, which incorporates intermolecular interactions forces which are modeled as a function of density following the work of van der Waals [20]. The exclusion volume effect of Enskog [21] is also incorporated to account for an increase in collision probability due to the increase in the density of nonideal fluids. These features naturally give rise to surface tension and phase segregation effects. The other variables which appear in the above equations will now be described. Π_{rr}, Π_{rz}, and Π_{zz} are the components of the viscous stress tensor and are given by

$$\Pi_{rr} = 2\mu\partial_r u_r, \tag{4}$$

$$\Pi_{rz} = \Pi_{zr} = \mu(\partial_z u_r + \partial_r u_z), \tag{5}$$

$$\Pi_{zz} = 2\mu\partial_z u_z, \tag{6}$$

where μ is the dynamic viscosity. $F_{s,r}$ and $F_{s,z}$ are the axial and radial components, respectively, of the surface tension force, which are given by [19]

$$F_{s,r} = \kappa\rho\partial_r\left[\frac{1}{r}\partial_r(r\partial_r\rho) + \partial_z(\partial_z\rho)\right], \tag{7}$$

$$F_{s,z} = \kappa\rho\partial_z\left[\frac{1}{r}\partial_r(r\partial_r\rho) + \partial_z(\partial_z\rho)\right], \tag{8}$$

where κ controls the strength of the surface tension force. This parameter is related to the surface tension of the fluid, σ, through the density gradient across the interface by the equation [22]

$$\sigma = \kappa\int\left(\frac{\partial\rho}{\partial n}\right)^2 dn. \tag{9}$$

Thus, the surface tension is a function of both the parameter κ and the density profile across the interface. The terms $F_{ext,r}$ and $F_{ext,z}$ in Eqs. (2) and (3), respectively, are the radial and axial components of external forces such as gravity.

The pressure P is related to density through the Carnahan–Starling–van der Waals equation of state (EOS) [23]

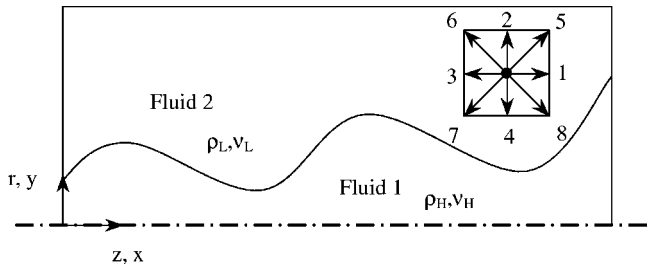

FIG. 1. Schematic of the arrangement of the coordinate system in axisymmetric multiphase flow [(r,z) and (y,x) coordinate directions are shown].

$$P = \rho RT\left\{\frac{1+\gamma+\gamma^2-\gamma^3}{(1-\gamma)^3}\right\} - a\rho^2, \tag{10}$$

where $\gamma = b\rho/4$. The parameter a is related to the intermolecular pairwise potential and b to the effective diameter of the molecule, d, and the mass of a single molecule, m, by $b = 2\pi d^3/3m$. R is a gas constant and T is the temperature. The Carnahan-Starling EOS has a *supernodal* $P-1/\rho-T$ curve—i.e., $dP/d\rho < 0$—for a certain range of values of ρ, when the state fluid temperature is below its critical value. This unstable part of the curve is the driving mechanism responsible for keeping the phases of fluids segregated and for maintaining a self-generated sharp interface.

We now modify the standard LBE in such a way that it effectively yields the axisymmetric multiphase flow equations (1)–(10) in a self-consistent way. To facilitate this, we employ the following coordinate transformation, illustrated in Fig. 1, which allows the governing equations to be represented in a Cartesian-like coordinate system—i.e., (x,y):

$$(r,z) \rightarrow (y,x), \tag{11}$$

$$(u_r,u_z) \rightarrow (u_y,u_x). \tag{12}$$

Assuming a summation convention for repeated subscript indices, Eqs. (1)–(8) may be transformed to

$$\partial_t\rho + \partial_k(\rho u_k) = -\frac{\rho u_y}{y}, \tag{13}$$

$$\rho(\partial_t u_i + u_k\partial_k u_i) = -\partial_i P + F_{s,i} + F_{ext,i} + \partial_k[\mu(\partial_k u_i + \partial_i u_k)] + F_{ax,i}, \tag{14}$$

where

$$F_{s,i} = \kappa\rho\partial_i\nabla^2\rho \tag{15}$$

and $i,j,k \in \{x,y\}$. The right-hand side (RHS) in Eq. (13), $-\rho u_y/y$, is the additional term in the continuity equation that arises from axisymmetry. The corresponding term for the momentum equation (14) is

$$F_{ax,i} = \frac{\mu}{y}[\partial_y u_i + \partial_i u_y] + \kappa\rho\partial_i\left(\frac{1}{y}\partial_y\rho\right). \tag{16}$$

To recover Eqs. (13) and (14), we introduce two additional source terms S'_α and S''_α to the standard 2D Cartesian LBE which has Ω_α as its collision term and a source term for

the internal and external forces, S_α. These unknown additional terms, representing the axisymmetric mass and momentum contributions, respectively, are to be determined so that the macroscopic behavior of the proposed LBE corresponds to axisymmetric multiphase flow. Thus, we propose the LBE

$$f_\alpha(\boldsymbol{x}+\boldsymbol{e}_\alpha\delta_t,t+\delta_t)-f_\alpha(\boldsymbol{x},t)=\frac{1}{2}[\,\Omega_\alpha|_{(x,t)}+\Omega_\alpha|_{(x+e_\alpha\delta_t,t+\delta_t)}] + \frac{1}{2}[\,S_\alpha|_{(x,t)}+S_\alpha|_{(x+e_\alpha\delta_t,t+\delta_t)}]\delta_t + \frac{1}{2}[\,S'_\alpha|_{(x,t)}+S'_\alpha|_{(x+e_\alpha\delta_t,t+\delta_t)}]\delta_t + \frac{1}{2}[\,S''_\alpha|_{(x,t)}+S''_\alpha|_{(x+e_\alpha\delta_t,t+\delta_t)}]\delta_t, \tag{17}$$

where f_α is the discrete single-particle distribution function, corresponding to the particle velocity e_α, where α is the velocity direction. The Cartesian component of the particle velocity, c, is given by $c=\delta_x/\delta_t$, where δ_x is the lattice spacing and δ_t is the time step corresponding to the two-dimensional, nine-velocity model (D2Q9) [24] shown in Fig. 1. Here, the collision term is given by the Bhatnagar-Gross-Krook (BGK) approximation [25]

$$\Omega_\alpha=-\frac{f_\alpha-f_\alpha^{eq}}{\tau},\quad \tau=\frac{\lambda}{\delta_t}, \tag{18}$$

where λ is the relaxation time due to collisions, δ_t is the time step, and f_α^{eq} is the truncated discrete form of the Maxwellian,

$$f_\alpha^{eq}\equiv f_\alpha^{eq,M}(\rho,\boldsymbol{u})=\omega_\alpha\left\{1+\frac{\boldsymbol{e}_\alpha\cdot\boldsymbol{u}}{RT}+\frac{(\boldsymbol{e}_\alpha\cdot\boldsymbol{u})^2}{2(RT)^2}-\frac{1}{2}\frac{\boldsymbol{u}\cdot\boldsymbol{u}}{RT}\right\}, \tag{19}$$

where R is the gas constant, T is the temperature, and w_α is the weighting coefficients in the Gauss-Hermite quadrature to represent the kinetic moment integrals of the distribution functions exactly [26]. For isothermal flows, the factor RT is related to the particle speed c as $RT=1/3c^2$. The term in Eq. (17),

$$S_\alpha=\frac{(e_{\alpha j}-u_j)(F_j+F_{ext,j})}{\rho RT}f_\alpha^{eq,M}(\rho,\boldsymbol{u}), \tag{20}$$

represents the effect of internal and external forcing terms on the change in the distribution function. The internal force term gives rise to surface tension and phase segregation effects which are given by

$$F_j=-\partial_j\psi+F_{s,j}, \tag{21}$$

where the function $\psi=P-\rho RT$ is the nonideal part of the equation of state, Eq. (10). The first two terms on the RHS of Eq. (17) corresponds to those presented by He *et al.* [27]. As mentioned above, the last two terms S'_α and S''_α in this equation are to be selected such that their behavior in the continuum limit would simulate the influence of the non-Cartesian-like terms in Eqs. (13) and (14) in a self-consistent way. Since the zeroth kinetic moment of the term $f_\alpha^{eq,M}(\rho,0)$ is involved in the derivation of the macroscopic mass conservation equation from the LBE, the source term S'_α in Eq. (17) is proposed to be equal to $f_\alpha^{eq,M}(\rho,0)$ multiplied by an unknown m' and normalized by the density ρ. The other source term S''_α is proposed analogous to the source term in Eq. (20). Thus, we propose

$$S'_\alpha=\frac{f_\alpha^{eq,M}(\rho,0)}{\rho}m', \tag{22}$$

$$S''_\alpha=\frac{(e_{\alpha j}-u_j)F''_j}{\rho RT}f_\alpha^{eq,M}(\rho,\boldsymbol{u}). \tag{23}$$

Here the unknowns m' and F''_j in the above two equations can be determined through Chapman-Enskog analysis as will be shown later. It must be stressed that all terms, including the collision term, on the RHS are discretized by the application of the trapezoidal rule, since it has been argued that at least a second-order treatment of the source terms is necessary for simulation of multiphase flow [10,11]. The macroscopic fields are given by

$$\rho=\sum_\alpha f_\alpha, \tag{24}$$

$$\rho u_i=\sum_\alpha f_\alpha e_{\alpha i}. \tag{25}$$

In this model, the order parameter is the density ρ, which distinguishes the different phases in the flow.

Equation (17) is implicit in time. To remove implicitness in this equation we introduce a transformation following the procedure described by He *et al.* [10,27], whereby

$$\overline{f}_\alpha=f_\alpha-\frac{1}{2}\Omega_\alpha-\frac{1}{2}(S_\alpha+S'_\alpha+S''_\alpha)\delta_t \tag{26}$$

in Eq. (17), so that we obtain

$$\overline{f}_\alpha(\boldsymbol{x}+\boldsymbol{e}_\alpha\delta_t,t+\delta_t)-\overline{f}_\alpha(\boldsymbol{x},t) = \overline{\Omega}_\alpha|_{(x,t)}+\frac{\tau}{\tau+1/2}[S_\alpha+S'_\alpha+S''_\alpha]|_{(x,t)}\delta_t, \tag{27}$$

where

$$\overline{\Omega}_\alpha=-\frac{\overline{f}_\alpha-f_\alpha^{eq}}{\tau+1/2}. \tag{28}$$

Thus, $\overline{f}_\alpha$ is the transformed distribution function that removes implicitness in the proposed LBE, Eq. (17), which describes the evolution of the f_α distribution function. The following constraints on the equilibrium distribution and the various source terms [28,29] are imposed from their definition:

$$\sum_\alpha f_\alpha^{eq} = \rho, \quad \sum_\alpha f_\alpha^{eq} e_{\alpha i} = \rho u_i, \quad \sum_\alpha f_\alpha^{eq} e_{\alpha i} e_{\alpha j} = \rho RT\delta_{ij} + \rho u_i u_j,$$

$$\sum_\alpha f_\alpha^{eq} e_{\alpha i} e_{\alpha j} e_{\alpha k} = \rho (RT)^2 (u_i \delta_{jk} + u_j \delta_{ki} + u_k \delta_{ij}), \tag{29}$$

$$\sum_\alpha S_\alpha = 0, \quad \sum_\alpha S_\alpha e_{\alpha i} = F_i,$$

$$\sum_\alpha S_\alpha e_{\alpha i} e_{\alpha j} = (F_i + F_{ext,i}) u_j + (F_j + F_{ext,j}) u_i, \tag{30}$$

$$\sum_\alpha S'_\alpha = m', \quad \sum_\alpha S'_\alpha e_{\alpha i} = 0, \quad \sum_\alpha S'_\alpha e_{\alpha i} e_{\alpha j} = m' RT\delta_{ij}, \tag{31}$$

$$\sum_\alpha S''_\alpha = 0, \quad \sum_\alpha S''_\alpha e_{\alpha i} = F''_i, \quad \sum_\alpha S''_\alpha e_{\alpha i} e_{\alpha j} = (F''_i u_j + F''_j u_i). \tag{32}$$

Then the following relationships are obtained between the transformed distribution function and the macroscopic fields, which also include the curvature effects resulting from axial symmetry:

$$\rho = \sum_\alpha \overline{f}_\alpha + \frac{1}{2} m' \delta_t, \tag{33}$$

$$\rho u_i = \sum_\alpha \overline{f}_\alpha e_{\alpha i} + \frac{1}{2} (F_i + F_{ext,i} + F''_i) \delta_t. \tag{34}$$

Now, to establish the unknowns m' and F''_j in the above formulation, the Chapman-Enskog multiscale analysis is performed [21]. Introducing the expansions [30]

$$\overline{f}_\alpha(\boldsymbol{x} + \boldsymbol{e}_\alpha \delta_t, t + \delta_t) = \sum_{\alpha=0}^{\infty} D_{t_n} \overline{f}_\alpha(\boldsymbol{x}, t), \tag{35}$$

$$D_{t_n} \equiv \partial_{t_n} + e_{\alpha k} \partial_k, \tag{36}$$

$$f_\alpha = \sum_{\alpha=0}^{\infty} \epsilon^n f_\alpha^{(n)}, \tag{37}$$

$$\partial_t = \sum_{\alpha=0}^{\infty} \epsilon^n \partial_{t_n}, \tag{38}$$

where $\epsilon = \delta_t$ in Eq. (27), and using Eq. (26) to transform $\overline{f}_\alpha$ back to f_α, the following equations are obtained in the consecutive order of the parameter ϵ:

$$O(\epsilon^0): f_\alpha^{(0)} = f_\alpha^{eq}, \tag{39}$$

$$O(\epsilon^1): D_{t_0} f_\alpha^{(0)} = -\frac{1}{\tau} f_\alpha^{(1)} + S_\alpha + S'_\alpha + S''_\alpha, \tag{40}$$

$$O(\epsilon^2): \partial_{t_1} f_\alpha^{(0)} + D_{t_0} f_\alpha^{(1)} = -\frac{1}{\tau} f_\alpha^{(2)}. \tag{41}$$

Now, invoking the Chapman-Enskog ansatz

$$\sum_\alpha \begin{pmatrix} 1 \\ e_{\alpha i} \end{pmatrix} f_\alpha^{(0)} = \begin{pmatrix} \rho \\ \rho u_i \end{pmatrix}, \quad \sum_\alpha \begin{pmatrix} 1 \\ e_{\alpha i} \end{pmatrix} f_\alpha^{(n)} = \begin{pmatrix} 0 \\ 0 \end{pmatrix}, \quad n \geqslant 1, \tag{42}$$

and performing $\Sigma_\alpha(\cdot)$ on Eqs. (40) and (41), we obtain

$$\partial_{t_0} \rho + \partial_k (\rho u_k) = m', \tag{43}$$

$$\partial_{t_1} \rho = 0, \tag{44}$$

respectively. Combining the first- and second-order results given by Eqs. (43) and (44) and considering $\partial_t = \partial_{t_0} + \epsilon \partial_{t_1}$, we get

$$\partial_t \rho + \partial_k (\rho u_k) = m'. \tag{45}$$

Comparing this equation and Eq. (13), the unknown m' is obtained as

$$m' = -\frac{\rho u_y}{y}. \tag{46}$$

This is the axisymmetric contribution to the Cartesian form of the equation for the order parameter—i.e., the density characterizing the different phases of the flow. Taking the first kinetic moment, $\Sigma_\alpha e_{\alpha i}(\cdot)$, of Eqs. (40) and (41), respectively, we get

$$\partial_{t_0} (\rho u_i) + \partial_k (\rho u_i u_k) = -\partial_i (\rho RT) + F_i + F_{ext,i} + F''_i, \tag{47}$$

$$\partial_{t_1} (\rho u_i) + \partial_k \Pi_{ij}^{(1)} = 0, \tag{48}$$

where

$$\Pi_{ij}^{(1)} = \sum_\alpha f_\alpha^{(1)} e_{\alpha i} e_{\alpha j}. \tag{49}$$

Employing the expression for $f_\alpha^{(1)}$ from Eq. (40) in Eq. (49), together with the summational constraints given above, and neglecting terms of the order $O(Ma^3)$ or higher, we get

$$\Pi_{ij}^{(1)} = -\tau RT\rho (\partial_j u_i + \partial_i u_j). \tag{50}$$

Equation (48) then simplifies to

$$\partial_{t_1} (\rho u_i) = \partial_j [\tau RT\rho (\partial_j u_i + \partial_i u_j)]. \tag{51}$$

Combining Eqs. (47) and (51), we get

$$\partial_t (\rho u_i) + \partial_k (\rho u_i u_k) = -\partial_i (\rho RT) + F_i + F_{ext,i} + F''_i + \partial_j [\tau \delta_t RT\rho (\partial_j u_i + \partial_i u_j)], \tag{52}$$

or substituting for F_i from Eq. (21), we obtain

$$\partial_t (\rho u_i) + \partial_k (\rho u_i u_k) = -\partial_i P + F_{s,i} + F_{ext,i} + F''_i + \partial_j [\tau \delta_t RT\rho (\partial_j u_i + \partial_i u_j)]. \tag{53}$$

Using Eqs. (45) and (53), this can be simplified to

$$\rho(\partial_t u_i + u_k \partial_k u_i) - \frac{\rho u_i u_y}{y} = -\partial_i P + F_{s,i} + F_{ext,i} + F_i'' + \partial_j[\tau \delta_t RT \rho(\partial_j u_i + \partial_i u_j)]. \tag{54}$$

Comparing Eqs. (14) and (54), we obtain the other unknown F_i'' where

$$F_i'' = F_{ax,i} - \frac{\rho u_i u_y}{y} = \frac{\mu}{y}[\partial_y u_i + \partial_i u_y] + \kappa \rho \partial_i \left(\frac{1}{y} \partial_y \rho \right) - \frac{\rho u_i u_y}{y}. \tag{55}$$

This is the axisymmetric contribution to the Cartesian form of the equation for the momentum, where the first, second, and third terms on the RHS correspond to the viscous, surface tension, and inertial force contributions, respectively. The dynamic viscosity is related to the relaxation time for collisions by $\mu = \rho \tau \delta_t RT = \rho \lambda c_s^2$, where $c_s^2 = 1/3c^2$. The set of equations corresponding to the axisymmetric LBE multiphase flow model is given by Eqs. (27) and (28) together with Eqs. (20), (22), (23), (33), (34), (46), and (55). In general, this multiphase model and that proposed by He *et al.* [10] face difficulties for fluids far from the critical point and/or in the presence of external forces. This difficulty is related to the calculation of the intermolecular force in Eq. (21), involving the computation of $\partial_j \psi$ which can become quite large across interfaces. Unless this term is accurately computed, the model may become unstable because of numerical errors [14,31]. Hence, an improved treatment of this term is necessary. This will now be described.

III. AXISYMMETRIC LBE MULTIPHASE FLOW MODEL WITH REDUCED COMPRESSIBILITY EFFECTS

He and co-workers [11] have proposed that through a suitable transformation of the distribution function f_α, which involves invoking the incompressibility condition of the fluid, and employing a new distribution function for capturing the interface, the difficulty with handling the intermolecular force term $\partial_j \psi$ can be reduced. We apply this idea to the axisymmetric model developed in the previous section. We replace the distribution function f_α by another distribution function g_α through the transformation [11]

$$g_\alpha = f_\alpha RT + \psi(\rho) \frac{f_\alpha^{eq,M}(\rho,0)}{\rho}. \tag{56}$$

The effect of this transformation will be discussed in greater detail below. By considering the fluid to be incompressible, i.e.,

$$\frac{d}{dt}\psi(\rho) = (\partial_t + u_k \partial_k)\psi(\rho) = 0, \tag{57}$$

and using the transformation, Eqs. (56) and (26), Eq. (27) is replaced by

$$\overline{g_\alpha}(\boldsymbol{x} + \boldsymbol{e}_\alpha \delta_t, t + \delta_t) - \overline{g_\alpha}(\boldsymbol{x}, t) = \overline{\Omega}_{g\alpha}|_{(x,t)} + \frac{\tau}{\tau + 1/2}[S_{g\alpha} + S'_{g\alpha} + S''_{g\alpha}]|_{(x,t)} \delta_t, \tag{58}$$

where

$$\overline{\Omega}_{g\alpha} = -\frac{\overline{g_\alpha} - g_\alpha^{eq}}{\tau + 1/2} \tag{59}$$

and

$$g_\alpha^{eq} = f_\alpha^{eq} RT + \psi(\rho) \frac{f_\alpha^{eq,M}(\rho,0)}{\rho}. \tag{60}$$

The corresponding source terms become

$$S_{g\alpha} = (e_{\alpha j} - u_j)\left[(F_j + F_{ext,j}) \frac{f_\alpha^{eq,M}(\rho,\boldsymbol{u})}{\rho} - \left(\frac{f_\alpha^{eq,M}(\rho,\boldsymbol{u})}{\rho} - \frac{f_\alpha^{eq,M}(\rho,0)}{\rho} \right) \partial_j \psi(\rho) \right], \tag{61}$$

$$S'_{g\alpha} = S'_\alpha RT = \frac{f_\alpha^{eq,M}(\rho,0)}{\rho} \left(-\frac{\rho u_y}{y} \right) RT, \tag{62}$$

$$S''_{g\alpha} = S''_\alpha RT = (e_j - u_j) F_j'' \frac{f_\alpha^{eq,M}(\rho,\boldsymbol{u})}{\rho}. \tag{63}$$

The term $\partial_j \psi$ in Eq. (61) is multiplied by the factor $[f_\alpha^{eq,M}(\rho,\boldsymbol{u})/\rho - f_\alpha^{eq,M}(\rho,0)/\rho]$. This factor, from the definition of the equilibrium distribution function f_α^{eq} in Eq. (19), is proportional to the Mach number and thus becomes smaller in the incompressible limit. Hence, it alleviates the difficulties associated with the calculation of the $\partial_j \psi$, a major source of numerical instability with the original model [10]. Thus, Eqs. (58)–(63) are found to be numerically more stable compared to Eq. (27) supplemented with Eqs. (20), (22), and (23). In this new framework, we still need to introduce an order parameter to capture interfaces. Here, we employ a function ϕ, referred to henceforth as the index function, in place of the density, as the order parameter to distinguish the phases in the flow.

The evolution equation of the distribution function whose emergent dynamics governs the index function has to be able to maintain phase segregation and mass conservation. To do this, we employ Eq. (27) together with Eqs. (20), (22), and (23) by keeping the term involving $\partial_j \psi$ and m', while the rest of the terms may be dropped as they play no role in mass conservation. In addition, the density is replaced by the index function in these equations. Hence, the evolution of the distribution function for the index function is given by

$$\overline{f_\alpha}(\boldsymbol{x} + \boldsymbol{e}_\alpha \delta_t, t + \delta_t) - \overline{f_\alpha}(\boldsymbol{x}, t) = \overline{\Omega}_{f\alpha}|(x,t) + \frac{\tau}{\tau + 1/2}[S_{f\alpha} + S'_{f\alpha}]|_{(x,t)} \delta_t, \tag{64}$$

where the collision and the source terms are given by

$$\overline{\Omega}_{f\alpha} = -\frac{\overline{f}_\alpha - \frac{\phi}{\rho} f_\alpha^{eq}}{\tau + 1/2}, \tag{65}$$

$$S_{f\alpha} = \frac{(e_j - u_j)(-\partial_j \psi(\phi))}{\rho RT} f_\alpha^{eq,M}(\rho, \boldsymbol{u}), \tag{66}$$

$$S'_{f\alpha} = \frac{\phi}{\rho} S'_\alpha = \frac{f_\alpha^{eq,M}(\rho,0)}{\rho}\left(-\frac{\phi u_y}{y}\right). \tag{67}$$

The hydrodynamic variables such as pressure and fluid velocity can be obtained by taking appropriate kinetic moments of the distribution function g_α—i.e.,

$$P = \sum_\alpha \overline{g}_\alpha - \frac{1}{2} u_j \partial_j \psi(\rho) + \frac{1}{2} m' RT \delta_t, \tag{68}$$

$$\rho RT u_i = \sum_\alpha \overline{g}_\alpha e_{\alpha i} + \frac{1}{2}(F_{s,i} + F_{ext,i})\delta_t + \frac{1}{2} F''_i \delta_t. \tag{69}$$

This follows from the definition of $\overline{g}_\alpha$ given in Eq. (56) and also includes curvature effects. The index function is obtained from the distribution function $\overline{f}_\alpha$ by taking the zeroth kinetic moment—i.e.,

$$\phi = \sum_\alpha \overline{f}_\alpha + \frac{1}{2}\frac{\phi}{\rho} m' \delta_t. \tag{70}$$

The terms m' and F''_i are given in Eqs. (46) and (55), respectively. The density is obtained from the index function through linear interpolation—i.e.,

$$\rho(\phi) = \rho_L + \frac{\phi - \phi_L}{\phi_H - \phi_L}(\rho_H - \rho_L), \tag{71}$$

where ρ_L and ρ_H are the densities of the light and heavy fluids, respectively, and ϕ_L and ϕ_H refer to the minimum and maximum values of the index function, respectively. These limits of the index function are determined from Maxwell's equal area construction [20] applied to the function $\psi(\phi) + \phi RT$.

Thus, the axisymmetric LBE multiphase flow model with reduced compressibility effects corresponds to Eqs. (58)–(71). The relaxation time for collisions is related to the viscosity of the fluid using the same expression as derived in the previous section. If the kinematic viscosity of the light fluid, ν_L, is different from that of the heavy fluid, ν_H, its value at any point in the fluid is obtained from the index function through linear interpolation—i.e.,

$$\nu(\phi) = \nu + \frac{\phi - \phi_L}{\phi_H - \phi_L}(\nu - \nu_L). \tag{72}$$

It may be seen that the model requires the calculation of spatial gradients in Eqs. (61) and (66) and of the Laplacian in Eq. (15). Since maintaining accuracy as well as isotropy is important for the surface tension terms, they are calculated by employing a fourth-order finite-difference scheme for the gradient and a second-order scheme for the Laplacian, given, respectively, by

$$\partial_i \varpi = \frac{1}{36\delta_x}\sum_{\alpha=1}^{8}[8\varpi(\boldsymbol{x} + \boldsymbol{e}_{\alpha i}\delta_t) - \varpi(\boldsymbol{x} + 2\boldsymbol{e}_{\alpha i}\delta_t)]\left(\frac{e_{\alpha i}}{c}\right) + O(\delta_t^4) \tag{73}$$

and

$$\nabla^2 \varpi \equiv \partial_i \partial_i \varpi = \frac{1}{3\delta_x^2}\sum_{\alpha=1}^{8}[\varpi(\boldsymbol{x} + \boldsymbol{e}_{\alpha i}\delta_t) - \varpi(\boldsymbol{x})] + O(\delta_x^2) \tag{74}$$

for any function ϖ. Notice that these discretizations are both based on the lattice based stencil, instead of the standard stencil based on the coordinate directions. In addition, in the application of this model, the implementation of boundary conditions plays an important role. In particular, along the axisymmetric line—i.e., $y=0$—specular reflection boundary conditions are employed for the distribution functions. For the D2Q9 model shown in the inset of Fig. 1, we set $\overline{f}_2 = \overline{f}_4$, $\overline{f}_5 = \overline{f}_8$, and $\overline{f}_6 = \overline{f}_7$ and $\overline{g}_2 = \overline{g}_4$, $\overline{g}_5 = \overline{g}_8$, and $\overline{g}_6 = \overline{g}_7$ for the distribution functions after the streaming step. For macroscopic conditions, along this line, $u_y = \partial_y(\cdot) = 0$, through which the singular source terms of type $1/y(\cdot)$ in the model can be appropriately treated. On the other hand, boundary conditions along the other lines are similar to those for the standard LBE.

IV. RESULTS AND DISCUSSION

In the rest of this paper, unless otherwise specified, the results are presented in lattice units; i.e., the velocities are scaled by the particle velocity c, the distance by the minimum lattice spacing δ_x, and time by c/δ_x. All other quantities are scaled as appropriate combinations of these basic units. First, the axisymmetric LBE multiphase flow models are applied to verify the well-known Laplace-Young relation for an axisymmetric drop. According to this relation, $\Delta P = 2\sigma/R_d$, where ΔP is the difference between the pressure inside and outside of a drop, σ is the surface tension, and R_d is the drop radius. For different choices of the surface tension parameter κ, the surface tension values are obtained from Eq. (9) by the replacing density in Eqs. (7) and (8) by the index function. To obtain the normal gradient used in Eq. (9), a physical configuration consisting of a liquid and a gas layer is set up. Once equilibrium is reached, the density gradient may be computed and hence the surface tension. Having obtained the relationship between the surface tension σ and the parameter κ, axisymmetric drops of four different radii $R_d = 40$, 50, 60, and 70 are set up in a domain discretized by 201×101 lattice sites. Periodic boundaries are considered in the x direction and an open boundary condition is considered along the boundary that is parallel to the axisymmetric boundary. By considering three different values of κ, 0.05, 1.0, and 0.15, the pressure difference across the drops is determined. Figure 2 shows a comparison of the pressure difference across the interface of the drops computed using the axisymmetric model developed in Sec. III and that predicted by the Laplace-Young relation. It is found that the computed results

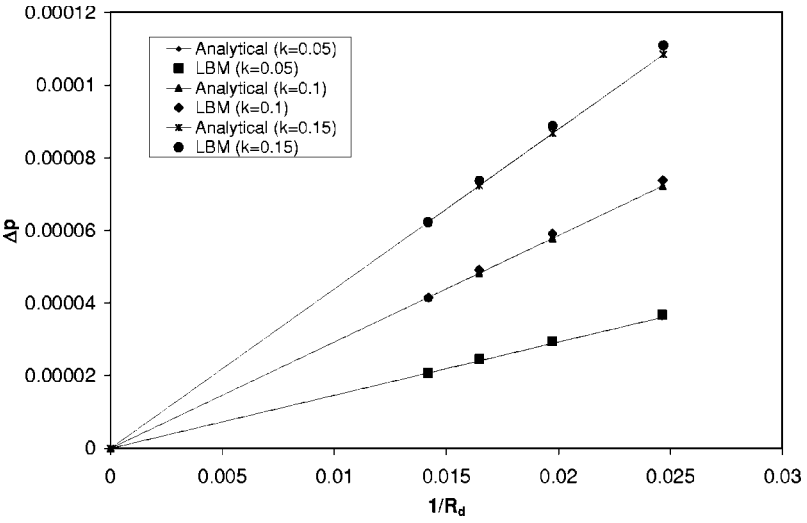

FIG. 2. Pressure difference across axisymmetric drops as a function of radius for different values of the surface tension parameter κ. Comparison of computed results using the axisymmetric LBE model versus theoretical prediction based on the Laplace-Young relation. Quantities are in lattice units.

are in good agreement with the theoretical values, with a maximum relative error of about 3%.

Another important test problem is that of an oscillating axisymmetric drop immersed in a gas. Since current versions of the LBE simulate a relatively viscous fluid, it is appropriate to compare the oscillation frequency with that of Miller and Scriven [32]. In contrast to earlier analytical solutions on drop oscillations, this work considers viscous dissipation effects in the boundary layer at the interface. According to [32], the frequency for the nth mode of oscillation for a drop is given by

$$\omega_n = \omega_n^* - \frac{1}{2}\alpha\omega_n^{*1/2} + \frac{1}{4}\alpha^2, \tag{75}$$

where ω_n is the angular response frequency and ω_n^* is Lamb's natural resonance frequency expressed as [33]

$$(\omega_n^*)^2 = \frac{n(n+1)(n-1)(n+2)}{R_d^3[n\rho_g + (n+1)\rho_l]}\sigma. \tag{76}$$

R_d is the equilibrium radius of the drop, σ is the interfacial surface tension, and ρ_l and ρ_g are the densities of the two fluids. The parameter α is given by

$$\alpha = \frac{(2n+1)^2(\mu_l\mu_g\rho_l\rho_g)^{1/2}}{2^{1/2}R_d[n\rho_g + (n+1)\rho_l][(\mu_l\rho_l)^{1/2} + (\mu_g\rho_g)^{1/2}]}, \tag{77}$$

where μ_l and μ_g are the dynamic viscosity of the two liquids. The subscripts g and l refer to the ambient gas and liquid phases, respectively. We consider the second mode of oscillation and analytical expressions for the time period are presented in Eq. (75).

The initial computational setup consists of a prolate spheroid of minimum (R_{min}) and maximum (R_{max}) radii of 40 and 55, respectively, placed in the center of the domain discretized by 201×101 lattice sites. We consider the surface tension parameters $\kappa=0.2$ and the density of the gas and the drop to be $\rho_g=0.1$ and $\rho_l=0.4$, respectively. The kinematic viscosities of both the gas and the drop are considered to be the same and given by $\nu_g=\nu_l=1.6667\times10^{-2}$. Figure 3 shows the configurations of an oscillating drop at different times computed using the standard axisymmetric model with these conditions. The drop changes from a prolate shape at $t=2000$ to oblate shape at $t=16\,000$. Such shape changes continue until the drop reaches its equilibrium spherical shape. Figure 4 shows the temporal evolution of the interface locations of the oscillating drop with the conditions above for two different surface tension parameters $\kappa=0.02$ and 0.08. It is expected that increasing the surface tension will reduce the time period of oscillations. The computed (T_{LBE}) and analytical (T_{anal}) time periods, where $T_{anal}=2\pi/\omega_2$, when $\kappa=0.02$ are 29 483 and 29 448, respectively. As κ is increased to 0.08, T_{TBE} and T_{anal} become 14 388 and 14 313, respectively. It may be seen that the computed and analytical values agree well, the difference being less than 1%. Also, the time period decreases as κ is increased, which is consistent with expectations.

Consider next the effect of changing the drop size on the time period of oscillations. Figure 5 shows the interface locations of an oscillating drop as a function of time for the following two initial sizes: $R_{min}=30$, $R_{max}=45$ and $R_{min}=40$, $R_{max}=55$. Reducing the drop size reduces its time period. The computed time period of the larger drop is equal to 29 483, while that for the smaller drop is 20 118. Comparison of the computed time periods with the analytical solution shows that they agree within 1% for these cases. Next, consider three different kinematic viscosities of the liquid: $\nu_l=1.6667\times10^{-2}$, 3.3333×10^{-2}, and 5.0×10^{-2}. Figure 6 shows the effect of drop viscosity on the temporal evolution of the interface locations of the drop. It is found that as the kinematic viscosity is increased the time period increases moderately which is consistent with the analytical solution. The computed time periods at these viscosities are 29 483, 31 030, and 32 925, while the analytical values are 29 448, 30 597, and 31 318, respectively, with a maximum error within 5.1%.

The third test problem considered here is that of the breakup of a cylindrical liquid column into drops, a fascinating problem of long-standing theoretical and practical interest. In a seminal work, Rayleigh [34] showed through a linear stability analysis of an inviscid column of cylindrical liquid of radius R_c that the column will be unstable if the axisymmetric wavelength of any disturbance λ_d is longer

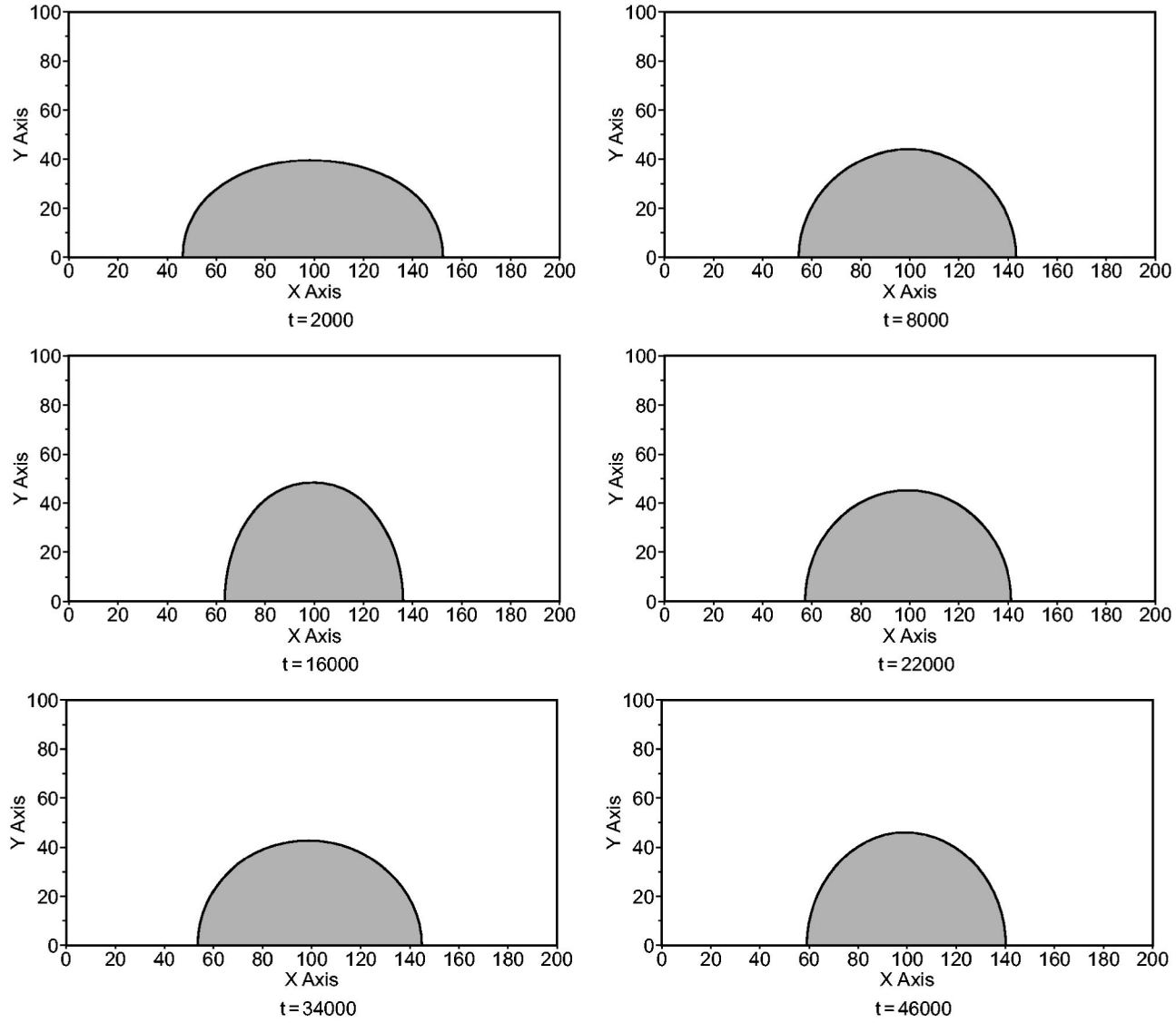

FIG. 3. Configurations of an oscillating drop as a function of time: $R_{min}=40$, $R_{max}=55$, $\rho_g=0.1$, $\rho_l=0.4$, and $\nu_l=\nu_g=1.6667\times10^{-2}$. Quantities are in lattice units.

than its circumference; i.e., the wave number $k^*=2\pi R_c/\lambda_d$ should be less than 1. Later, the theoretical analysis was extended to more realistic conditions by including viscosity. In the last three decades, several experimental and numerical investigations have also been performed. To evaluate the axisymmetric LBE model, we study the Rayleigh capillary instability for different wave numbers. Initial studies carried out with $k^*>1$ showed that the liquid does not break up. We will now present results of cases with break up. Consider a cylindrical liquid column of radius $R_c=45$ subject to an axisymmetric cosinusoidal wavelength $\lambda_d=320$—i.e., $k^*=0.88$. To simulate the dynamics of instability for this wave number, we consider a domain discretized by 321×151 lattice sites with $\rho_g=0.1$, $\rho_l=0.4$, $\nu_g=\nu_l=6.6667\times10^{-2}$, and $\kappa=0.1$. Since $k^*<1$, it is expected that the liquid column would eventually break up. Figure 7 shows the configurations of the liquid column at different times. As time progresses, the imposed interfacial disturbances on the liquid column grow. At $t=28\,000, 46\,000, 52\,000$, the cross section of the column becomes progressively thinner in the center, and by mass conservation, the ends becomes larger. At $t=60\,000$, notice that a bead-type structure is formed at the ends and with a thin ligament between them. Such a structure has been observed in experiments [1] and in other numerical simulations [35]. Eventually, the column breaks up, forming a thin ligament in the middle, which then becomes a satellite droplet.

Let us now increase the wavelength of the disturbance to $\lambda_d=600$, keeping the physical parameters the same as before. We consider a domain represented by 601×151 lattice sites. Since $R_c=45$, as before, the wave number is 0.47. Figure 8 shows the temporal evolution of the configurations of the liquid column at this reduced wave number. The axisymmetric disturbance grows with time. Since the wavelength is longer, it can be noticed that the ligament that is formed during the Rayleigh instability is also longer. As a result, after the column breaks up, a larger satellite droplet is

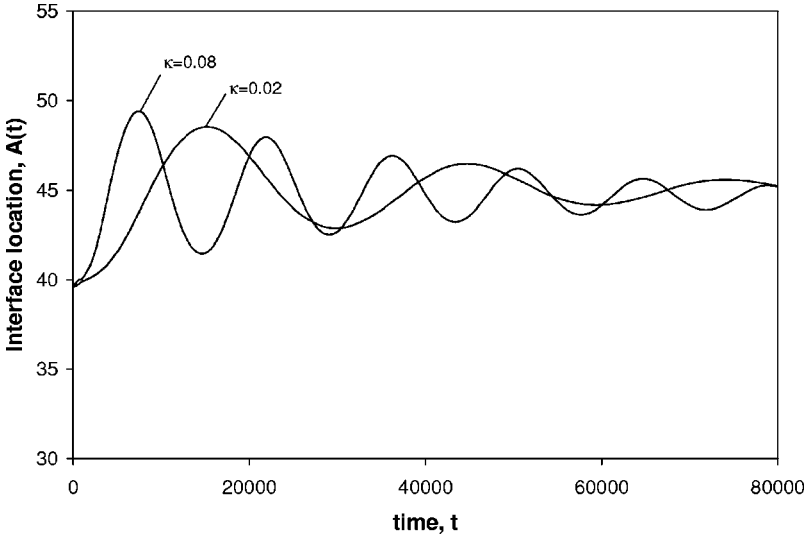

FIG. 4. Interface location of an oscillating drop as a function of time for two values of the surface tension parameter κ: $R_{min}=40$, $R_{max}=55$, $\rho_g=0.1$, $\rho_l=0.4$, and $\nu_l=\nu_g=1.6667\times10^{-2}$. Quantities are in lattice units.

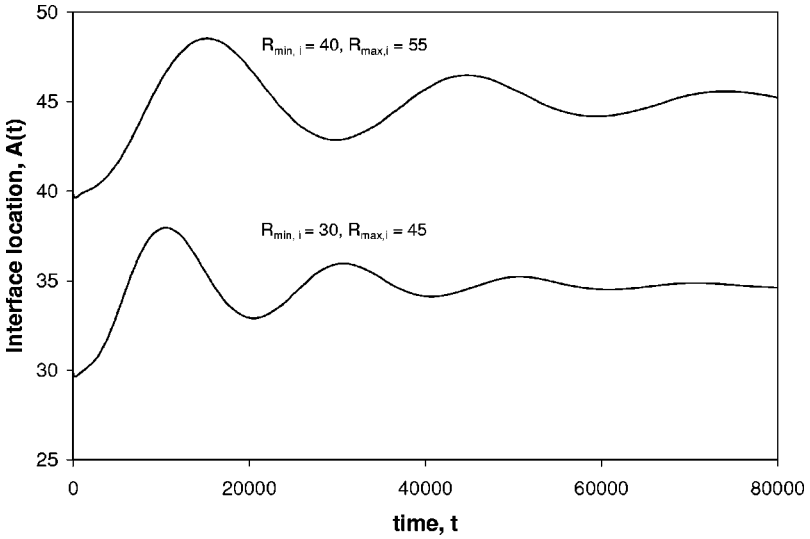

FIG. 5. Interface location of an oscillating drop as a function of time for two drop sizes: $\rho_g=0.1$, $\rho_l=0.4$, $\nu_l=\nu_g=1.6667\times10^{-2}$, and $\kappa=0.02$. Quantities are in lattice units.

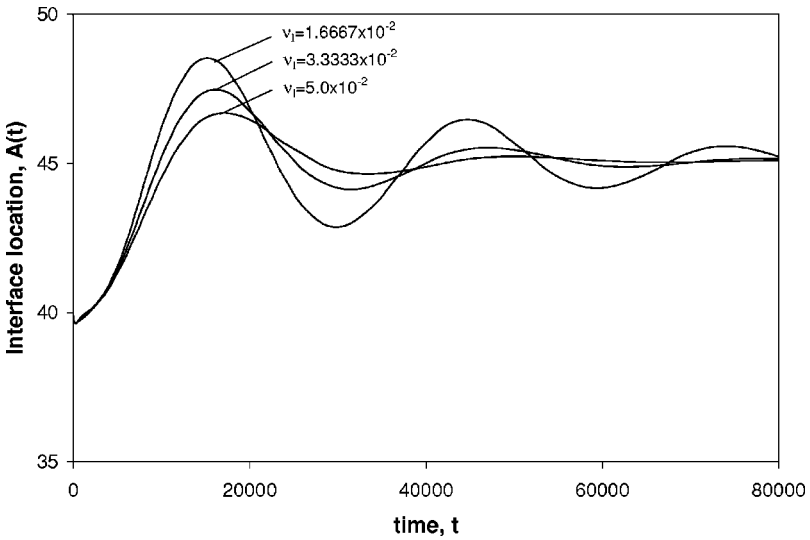

FIG. 6. Interface location of an oscillating drop as a function of time for different kinematic viscosities ν_l: $R_{min}=40$, $R_{max}=55$, $\rho_g=0.1$, $\rho_l=0.4$, and $\kappa=0.02$. Quantities are in lattice units.

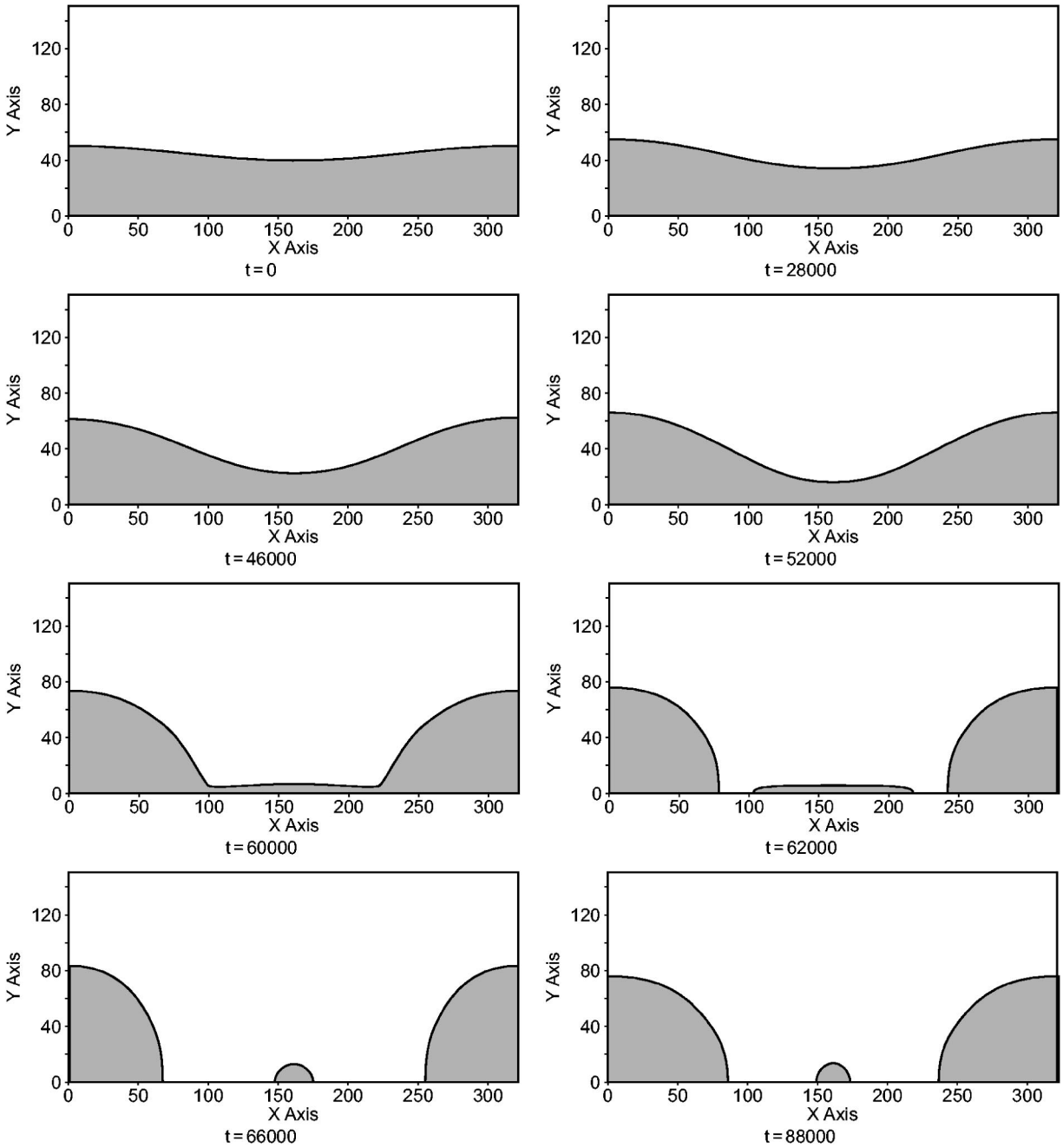

FIG. 7. Configurations of a cylindrical liquid column at different times undergoing Rayleigh breakup and satellite droplet formation: $k^*=0.88$, $\rho_g=0.1$, $\rho_l=0.4$, and $\nu_l=\nu_g=6.6667\times10^{-2}$. Quantities are in lattice units.

formed. To express the drop size distribution with wave numbers more quantitatively, we plot the nondimensional size of the main and satellite drops, $r^*=R/R_c$, as a function of wave number, k^* in Fig. 9. It may be noted that Rayleigh's original analysis predicts only the onset of breakup and not the formation of satellite droplets. To predict analytically satellite droplet formation, it has been shown that at least a third-order perturbation analysis of the Navier-Stokes equation (NSE) is needed [36]. Computations based on direct solutions of the NSE also predict the formation of the satellite droplets.

To evaluate the drop size distribution computed using the axisymmetric LBE model, we consider the experimental data of Rutland and Jameson [37], the experimental data and analytical solution based on a third-order perturbation analysis of the NSE by Lafrance [36], a boundary integral solution of the NSE by Mansour and Lundgren [38] and a finite-element solution of the NSE by Ashgriz and Mashayek [35]. It can be seen in the figure that as long as the wave number is less than 1, as expected there will be a satellite droplet formation. As the wave number is reduced, the sizes of both the main drop and satellite droplet increase. The rate of increase of the size

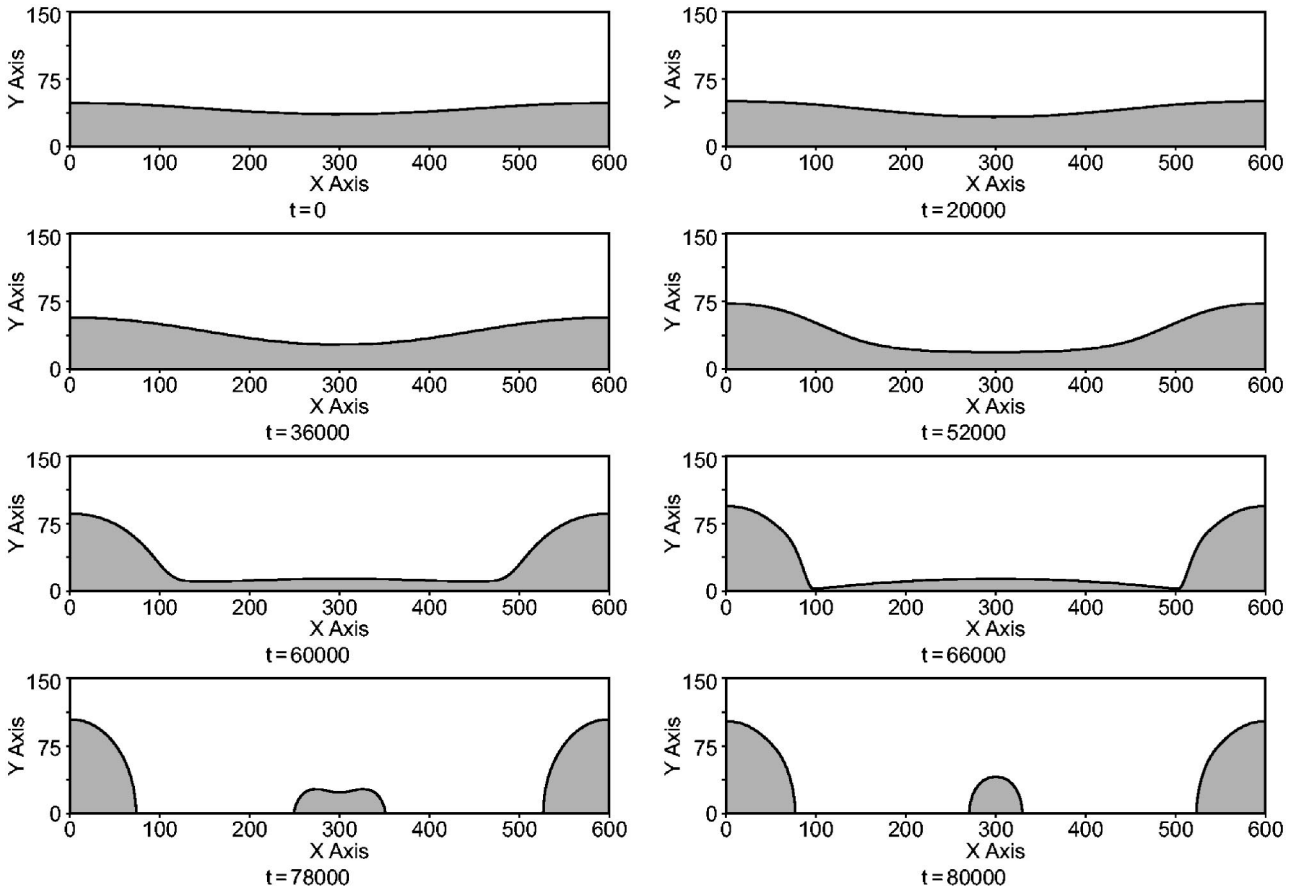

FIG. 8. Configurations of a cylindrical liquid column at different times undergoing Rayleigh breakup and satellite droplet formation: $k^*=0.47$, $\rho_g=0.1$, $\rho_l=0.4$, and $\nu_l=\nu_g=6.6667\times10^{-2}$. Quantities are in lattice units.

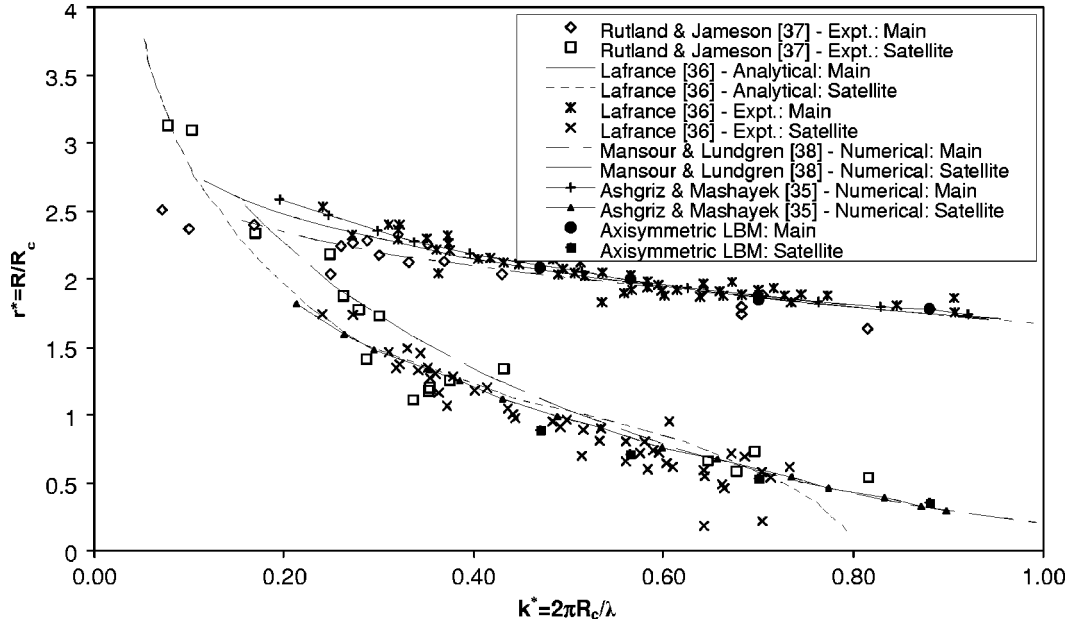

FIG. 9. Drop sizes resulting from Rayleigh breakup of liquid cylindrical column as a function of wave number k^*. Quantities are dimensionless.

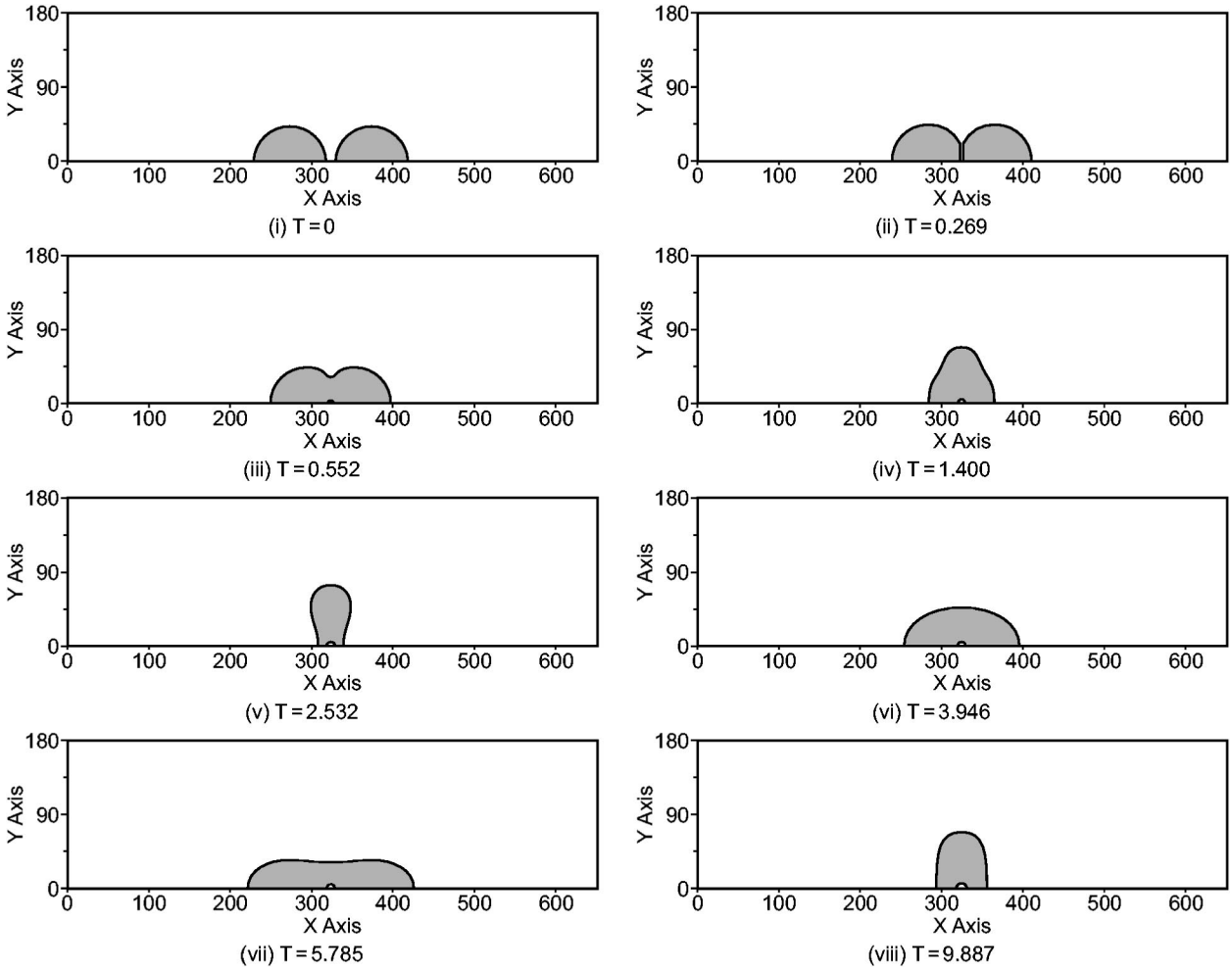

FIG. 10. Colliding drops at different times T: $N_{We}=20$, $N_{Oh}=0.589$, $r=4$, and $\lambda=1$. Time is normalized by the relative velocity between the drops and their diameter. Axes are in lattice units.

of the satellite droplet is greater than that of the main drop. Notice that there is considerable scatter in the available data in the figure. The computed results from the axisymmetric LBE model are presented for wave numbers greater than or equal to 0.47. Ignoring the two experimental data points of Lafrance [36] for the satellite drop sizes that deviate considerably from the others, we find that the axisymmetric model is able to reproduce the drop size distribution quantitatively within 12%.

The axisymmetric model has been employed to study head-on collisions of drops of radii R_1 and R_2 approaching each other with a relative velocity U. The dynamics and outcome of colliding drops are characterized mainly by the Weber number N_{We} defined by $N_{We}=\rho_l(R_1+R_2)U^2/\sigma$ [39]. Additional parameters that may have an influence are the Ohnesorge number N_{Oh} defined by $N_{Oh}=16\mu_l/\sqrt{\rho_l R_1 \sigma}$ and ratios of liquid and gas densities (r) and dynamic viscosities (λ). According to experiments [39], it is expected that lower N_{We} collisions lead to coalescence while higher N_{We} to separation by reflexive action. Figures 10 and 11 present drop configurations at $N_{We}=20$ and 100, respectively. Notice that at $N_{We}=20$, the drops coalesce, while at $N_{We}=100$, they eventually separate with the formation of a satellite droplet, which are consistent with experimental observations. Also notice that for the latter case, the temporarily coalesced drop undergoes various stages of deformation which are consistent with a recent theoretical analysis [40]. Additional details of these and other studies of drop collisions are given in Ref. [41].

V. SUMMARY

In this paper, a LB model for axisymmetric multiphase flows is developed. The axisymmetric model is developed by adding source terms to the standard Cartesian BGK LBE. The source terms, which are temporally and spatially dependent, represent the axisymmetric contributions of the order parameter, which distinguish the different phases, as well as inertial, viscous, and surface tension forces. Consistency of the model in achieving the desired axisymmetric flow multiphase behavior is established through the Chapman-Enskog multiscale analysis. The analysis shows that the axisymmetric macroscopic conservation equations are recovered in the continuum limit. An axisymmetric model with reduced com-

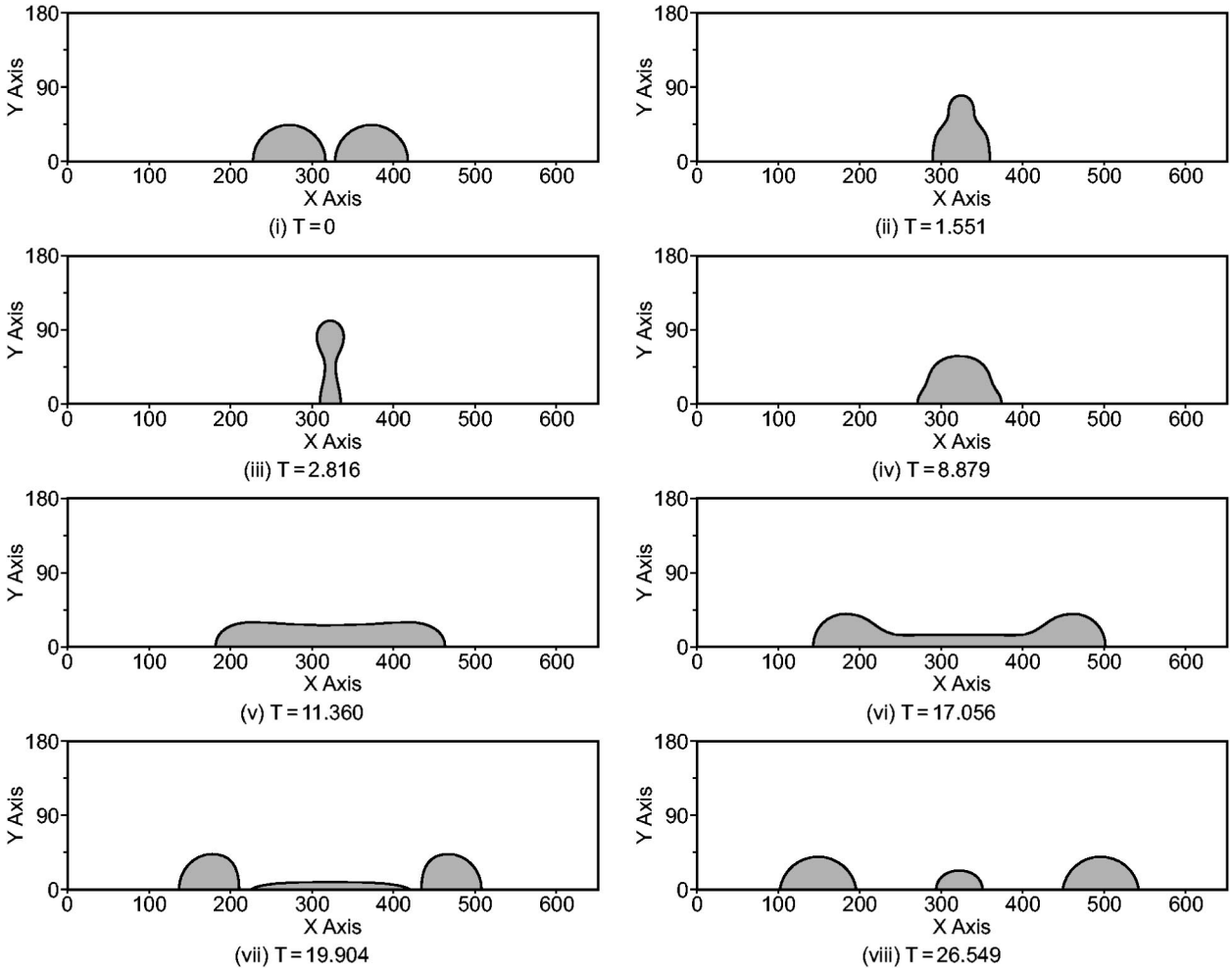

FIG. 11. Colliding drops at different times T: $N_{We}=100$, $N_{Oh}=0.589$, $r=4$, and $\lambda=1$. Time is normalized by the relative velocity between the drops and their diameter. Axes are in lattice units.

pressibility effects is then developed to improve its computational stability. In this version, a transformation is introduced to the distribution function in the LBE such that it reduces the compressibility effects. Comparisons of computed axisymmetric equilibrium drop formation and oscillations, Rayleigh capillary instability, breakup and formation of satellite drops liquid cylindrical liquid columns, and the outcomes of head-on drop collisions with available data show satisfactory agreement. The maximum error for the frequency of drop oscillations is less than 5.1% and that for drop sizes as a result of Rayleigh breakup is 12%.

ACKNOWLEDGMENTS

The authors thank Dr. X. He for helpful discussions and the Purdue University Computing Center (PUCC) and the National Center for Supercomputing Applications (NCSA) for providing access to computing resources.

[1] J. Eggers, Rev. Mod. Phys. **69**, 865 (1997).
[2] J. Hyman, Physica D **12**, 396 (1984).
[3] R. Scardovelli and S. Zaleski, Annu. Rev. Fluid Mech. **31**, 567 (1999).
[4] S. Chen and G. Doolen, Annu. Rev. Fluid Mech. **8**, 2527 (1998).
[5] S. Succi, I. Karlin, and H. Chen, Rev. Mod. Phys. **74**, 1203 (2002).
[6] X. Shan and H. Chen, Phys. Rev. E **47**, 1815 (1993).
[7] X. Shan and H. Chen, Phys. Rev. E **49**, 2941 (1994).
[8] M. Swift, W. Obsborn, and J. Yeomans, Phys. Rev. Lett. **75**, 830 (1995).
[9] M. Swift, S. Orlandini, W. Obsborn, and J. Yeomans, Phys. Rev. E **54**, 5041 (1996).
[10] X. He, X. Shan, and G. Doolen, Phys. Rev. E **57**, R13 (1998).
[11] X. He, S. Chen, and R. Zhang, J. Comput. Phys. **152**, 642 (1999).
[12] X. He and G. Doolen, J. Stat. Phys. **107**, 112 (2002).

[13] M. Sussman and P. Smereka, J. Fluid Mech. **341**, 269 (1996).
[14] X. He, R. Zhang, and G. Doolen, Phys. Fluids **11**, 1143 (1999).
[15] T. Inamuro, R. Tomita, and F. Ogino, Int. J. Mod. Phys. B **17**, 21 (2003).
[16] K. Premnath and J. Abraham, Int. J. Mod. Phys. C **16**, 25 (2005).
[17] I. Halliday, L. Hammond, C. Care, K. Good, and A. Stevens, Phys. Rev. E **64**, 011208 (2001).
[18] B. Nadiga and S. Zaleski, Eur. J. Mech. B/Fluids **15**, 885 (1996).
[19] Q. Zou and X. He, Phys. Rev. E **59**, 1253 (1999).
[20] J. Rowlinson and B. Widom, *Molecular Theory of Capillarity* (Clarendon Press, Oxford, 1982).
[21] S. Chapman and T. Cowling, *Mathematical Theory of Non-Uniform Gases* (Cambridge University Press, London, 1964).
[22] R. Evans, Adv. Phys. **28**, 143 (1979).
[23] N. Carnahan and K. Starling, J. Chem. Phys. **51**, 635 (1969).
[24] Y. Qian, D. d'Humières, and P. Lallemand, Europhys. Lett. **17**, 479 (1992).
[25] P. Bhatnagar, E. Gross, and M. Krook, Phys. Rev. **94**, 511 (1954).
[26] X. He and L.-S. Luo, Phys. Rev. E **55**, R63333 (1997).
[27] X. He, S. Chen, and G. Doolen, J. Comput. Phys. **146**, 282 (1998).
[28] L.-S. Luo, Phys. Rev. E **62**, 4982 (2000).
[29] Z. Guo, C. Zheng, and B. Shi, Phys. Rev. E **65**, 046308 (2002).
[30] X. He and L.-S. Luo, J. Stat. Phys. **88**, 927 (1997).
[31] X. He (private communication).
[32] C. Miller and L. Scriven, J. Fluid Mech. **32**, 417 (1968).
[33] H. Lamb, *Hydrodynamics* (Cambridge University Press, London, 1932).
[34] L. Rayleigh, Proc. London Math. Soc. **10**, 4 (1878).
[35] N. Ashgriz and F. Mashayek, J. Fluid Mech. **291**, 163 (1995).
[36] P. Lafrance, Phys. Fluids **18**, 428 (1975).
[37] D. Rutland and G. Jameson, J. Fluid Mech. **46**, 267 (1971).
[38] N. Mansour and T. Lundgren, Phys. Fluids A **2**, 1141 (1990).
[39] J. Qian and C. Law, J. Fluid Mech. **331**, 59 (1997).
[40] I. Roisman, Phys. Fluids **16**, 3438 (2004).
[41] K. NandhaPremnath and J. Abraham, Ph.D. thesis, Purdue University (2004).